HHS Public Access

Author manuscript

Neuroimage. Author manuscript; available in PMC 2018 February 01.

Published in final edited form as:

Neuroimage. 2017 February 01; 146: 288–292. doi:10.1016/j.neuroimage.2016.11.047.

Manual segmentation of the human bed nucleus of the stria terminalis using 3T MRI

Justin D. Theiss, BS, **Caitlin Ridgewell, MPH**, **Maureen McHugo, PhD**, **Stephan Heckers, MD**, and **Jennifer Urbano Blackford, PhD***

Department of Psychiatry and Behavioral Sciences, Vanderbilt University Medical Center, 1601 23rd Avenue South, Nashville, TN 37212, USA

Abstract

The bed nucleus of the stria terminalis (BNST)—a small gray matter region located in the basal forebrain—has been implicated in both anxiety and addiction based on compelling evidence from rodent and non-human primate studies. However, the BNST's small size and proximity to other gray matter regions has hindered non-invasive study in human subjects using standard neuroimaging methods. While initial studies have benefitted from a BNST mask created from a single human subject using a 7T scanner, individual variability is likely—especially in patient populations—thus a manual segmentation protocol is needed. Here we report on the development of a reliable manual segmentation protocol performed on 3T MRI images using a scanning sequence that provides high gray matter/white matter/cerebrospinal fluid contrast. Inter- and intra-rater reliabilities, measured in 10 healthy individuals, demonstrate that the protocol can be reliably implemented (intra-rater Dice similarity coefficient ≥ 0.85, inter-rater ≥ 0.77). This BNST tracing protocol provides the necessary foundation for future 3T MRI studies of the BNST in healthy controls and patient populations.

Keywords

BNST; anxiety; addiction; segmentation; MRI; volumes

1. INTRODUCTION

The bed nucleus of the stria terminalis (BNST) has received an increasing amount of interest in the past decade based on animal studies highlighting the BNST's critical role in both anxiety and addiction (Avery et al., 2016). Seminal rodent studies established that lesions of the BNST reduce sustained fear behaviors resulting from diffuse or unpredictable cues and contexts, akin to human anxiety (Davis et al., 2010, 1997; Shackman and Fox, 2016; Walker et al., 2003). Animal models of drug use, withdrawal, and reinstatement have demonstrated

*Corresponding author. Jennifer Urbano Blackford, PhD, Vanderbilt University Medical Center, Department of Psychiatry and Behavioral Sciences, 1601 23rd Avenue South, Suite 3057J. Tel.: 615.343.0715. Jennifer.blackford@vanderbilt.edu.

the BNST's involvement in each of these phases of addiction (Jennings et al., 2013; Kash, 2012; Koob and Volkow, 2010; Stamatakis et al., 2014) These compelling findings from animal models of anxiety and addiction have spurred interest in studying the BNST in humans.

Initial functional magnetic resonance imaging (fMRI) investigations of BNST function in humans have provided preliminary evidence that: the BNST is activated during anticipation of threat or reward loss (Alvarez et al., 2011; Grupe et al., 2013; Herrmann et al., 2016; Klumpers et al., 2015; Mcmenamin et al., 2014; Mobbs et al., 2010; Schlund et al., 2013); BNST activation is correlated with anxiety (Choi et al., 2012; Somerville et al., 2013, 2010) and childhood physical abuse (Banihashemi et al., 2013); and BNST activation is heightened in individuals with anxiety disorders (Münsterkötter et al., 2015; Straube et al., 2007; Yassa et al., 2012). Two recent papers provide thorough reviews of BNST fMRI findings in humans (Avery et al., 2016; Shackman and Fox, 2016).

Human neuroimaging studies of the BNST have been challenging due to the BNST's small size—about the size of a sunflower seed—and limitations of neuroimaging technology. For example, a recent meta-analysis (Avery et al., 2016) demonstrated that the lack of an anatomical delineation of the human BNST has made it challenging to determine whether regions that show activation in fMRI studies truly encompass the BNST. Several studies report using a BNST region of interest defined on a 3 Tesla (3T) structural MRI (Alvarez et al., 2011; Banihashemi et al., 2013; Herrmann et al., 2016; Mcmenamin et al., 2014; Motzkin et al., 2015). While the use of BNST masks has been an important step forward, the gray matter/white matter/cerebrospinal fluid contrast afforded by standard 3T structural MRIs is typically insufficient to identify the anterior and posterior boundaries of the BNST.

Two recent studies have made significant advances using ultra-high field 7T structural imaging. First, our lab used a combination of a 7T MRI and a novel GRASE sequence to anatomically localize the BNST on a single subject. The BNST mask was normalized to a standard MNI space and then mapped onto 90 subjects in order to identify the BNST's structural and functional connectivity using diffusion tensor imaging and resting-state fMRI at 3T at 3T (Avery et al., 2014). The functional connectivity pattern observed in this first study was replicated shortly after by McMenamin and colleagues (2014). The following year, Torrisi and colleagues (2015) used 7T T1 structural images to manually segment the BNST of 36 subjects and examine functional connectivity using 7T resting-state fMRI. Importantly, the functional connectivity observed at 7T largely also replicated the connectivity patterns observed at 3T.

While these studies provide compelling evidence that it is possible to anatomically delineate the human BNST using either GRASE or T1 7T scans, the number of 7T scanners is limited and the high number of safety exclusions for 7T MRI makes scanning patient populations-- such as elderly patients and combat Veterans-- nearly impossible. Furthermore, patient groups with well-established anatomical variability, for example enlarged ventricles in patients with schizophrenia, highlight the need for an anatomical delineation of the human BNST at 3T. Here, we report on the development of a reliable method for anatomically

delineating the human BNST using a short (4-min) T2-weighted sequence collected on a 3T MRI scanner.

2. MATERIALS AND METHODS

2.1 Participants

We selected T2-weighted images of 10 healthy participants from an ongoing study. Scans were selected based on the following criteria: absence of current and lifetime psychiatric disorders, as determined by the Structured Clinical Interview for the DSM-IV (First et al., 2002); free from psychotropic medications (within the past six months); and without significant scan artifacts, as visually inspected by JUB. Participants included in the analysis were 18–29 years old (mean ± SD: 23.4 ± 3.4), 40% female, and 90% right-handed. The participants were mostly Caucasian (90%; 10% African-American). The Vanderbilt University Institutional Review Board approved the study, and written consent was obtained prior to participation.

2.2 MRI scan acquisition

Scans were initially collected using a 3T Phillips Intera Achieva MRI scanner (Phillips Medical Systems, Andover, MA). A T2-weighted turbo spin-echo (TSE) sequence was collected based on the sequence developed by Yushkevich and colleagues (2010), consisting of 1 dynamic collected over 26 slices (480 × 480 matrix, voxel size = 0.479 mm × 0.479 mm × 2 mm, no gap, TR = 2380 ms, and TE = 90 ms). T2-weighted scans were coregistered with each subject's corresponding T1-weighted scan, which scaled voxel size to 0.8 mm × 0.8 mm × 0.9 mm.

2.3 BNST Delineation

The anatomical location and boundaries of the BNST were identified based on the Mai human brain atlas (Figure 1; Mai, Maijtanik, & Paxinos, 2015), which includes information from histological preparations and provides excellent detail for the delineation of subcortical structures. The BNST was initially traced in the coronal view, with the axial and sagittal views used for confirmation. In the coronal view, the inferior boundary was defined by the superior aspect of the anterior commissure. The superior boundary was defined by the thalamostriate vein when visible, or alternatively, the most ventral aspect of the caudate body. The medial and lateral boundaries were defined by the fornix and internal capsule, respectively. The anterior boundary of the BNST was defined as two slices or 1.8 mm anterior to the most anterior slice in which the anterior commissure is still visibly joined at the midline (see Supplemental Figure). Finally, the posterior boundary was defined by the interventricular foramen (see Supplemental Figure), the channel that forms between the lateral ventricles and third ventricle and is bordered by the fornix and the thalamus.

2.4 Manual Segmentation Protocol

The BNST was manually traced using 3DSlicer (version 4.5; www.slicer.org; Fedorov et al., 2012), a software package that provides simultaneous visualization in all orientations. Using 3DSlicer provided several advantages for tracing the BNST. The image contrast was modified so that BNST boundaries were definable consistently across raters. Each

hemisphere, beginning with the left, was segmented in the coronal view, with axial and sagittal views used for boundary refinement. Finally, in each view, the interpolated image was used for tracing and then the non-interpolated/raw image was used to exclude white matter and CSF.

After setting the appropriate image contrast, the interpolated view was selected for the tracing process. Each hemisphere was traced separately, starting with the left side as displayed in 3D Slicer. To provide a common starting point, all tracing began on the coronal slice in which the anterior commisure was most visible. All contiguous gray matter voxels were then traced within the defined boundaries. Tracing proceeded anteriorly to the anterior boundary and then posteriorly from the initial anterior commisure slice.

Once all coronal slices had been traced, the verification process began with the non-interpolated view, which provided clear identification of voxels to exclude as white matter or cerebrospinal fluid. Additionally, if it was not immediately apparent whether a voxel should be excluded or not, the image intensity values were used to exclude a voxel based on percent differences greater than 25% compared to a known, contiguous gray matter. After excluding cerebrospinal fluid and white matter voxels in each view, the axial view was utilized to verify inferior and superior boundaries using the interpolated view. Proceeding inferiorly in the axial view, the inferior boundary was verified by the first slice in which the anterior commisure appears. Proceeding superiorly in the axial view, the superior boundary was verified by the most inferior slice that included a clearly visible thalamostriate vein. In the case of more than one vein traversing this area, the most prominent vein was used to determine the boundary. However, if no thalamostriate vein was visible, the superior boundary was defined as being below the most inferior aspect of the caudate. Moving to the sagittal view, and proceeding medially, the medial boundary was verified by the first medial slice containing the fornix column. Also in the sagittal view, the lateral boundary was verified by the most lateral slice in which there was no longer contiguous gray matter and the lateral ventricle receded from view superiorly. For each of the above boundaries, all voxels contained within the boundary slice and exterior to it were excluded.

2.5 Reliability analysis

Fourteen T2-weighted scans (10 unique scans, 4 duplicate scans) were traced independently by JDT (Rater 1) and CRR (Rater 2) with completion times and image contrast parameters recorded. Rater 1 was the expert tracer and trained Rater 2 using the manual segmentation protocol until proficient. Since the BNST is a small and variable region, we used the Dice similarity coefficient (Dice, 1945) as the reliability measure. The Dice similarity coefficient is an apt measure in this case since the calculation is based on physical overlap at each voxel, providing the most stringent test of reliability in anatomical location. Inter- and intra-rater Dice similarity coefficients were calculated for left and right hemispheres separately. To determine whether individual rater factors influenced reliability, we tested the effect of between-rater differences in completion time and image contrast parameters on Dice coefficients with a multiple linear regression.

Next, we created a probabilistic mask using the 10 original scans traced by Rater 1. The T1 image from each subject was normalized to the MNI 152 1mm template using an initial

affine registration with the correlation ratio cost function and trilinear interpolation in FSL (Jenkinson and Smith, 2001) followed by a diffeomorphic registration using the SyN algorithm and BSpline interpolation in ANTs (Avants et al., 2008). Successful normalization was achieved without bias field correction. The parameters from the affine and diffeomorphic registrations were then applied to the BNST tracing using nearest neighbor interpolation in FSL followed by MultiLabel interpolation in ANTs. Next, tracings were averaged together to create the probabilistic mask (available at Neurovault.org). In order to provide a consistent volume that could be compared across laboratories in MNI space, these normalized tracings were used in determining average volume of the BNST. Finally, to determine whether manual tracings at 3T are a valid proxy for manual segmentation of images collected at 7T, we compared the 3T probabilistic mask to the previously published 7T single subject mask (Avery et al., 2014).

3. RESULTS

The average human BNST in our sample was 65.9 mm^3 (SD = 21.8) for the left hemisphere and 66.9 mm^3 (SD = 20.1) for the right hemisphere. Intra-rater Dice coefficients were excellent for both raters (Rater 1: 0.95 ± 0.05, right: 0.95 ± 0.05; Rater 2: left: 0.85 ± 0.04, right: 0.92 ± 0.03), indicating that this protocol can be used to reliably trace the anatomical boundaries of the BNST. Inter-rater Dice coefficients between raters were also very good (left: 0.79 ± 0.09, right: 0.77 ± 0.07). The inter-rater differences were largely due to slightly larger BNST tracings by Rater 2 compared to Rater 1 (left: $F(1, 12) = 11.2$, $p = 0.006$; right: $F(1, 12) = 16.2$, $p = 0.002$) but were not related to between-rater differences in completion time nor image contrast parameters (left: $F(3, 10) = 0.48$, $p = 0.70$; right: $F(3, 10) = 2.16$, $p = 0.16$).

Next, to determine the most appropriate mask for standard space use, the probabilistic mask (based on the 10 scans traced by Rater 1) was set at overlap thresholds of 10%, 25%, 50%, and 75%. The volumes of the left and right BNST at each threshold were averaged together for comparison to mean volume of the 7T BNST mask. The mean volumes for the different thresholds varied substantially from one another: 10% = 177 mm^3, 25% = 91 mm^3, 50% = 57 mm^3, and 75% = 31.5 mm^3. As a reference point, the original 7T BNST mask was 180 mm^3. It should be noted that these volumes include spatial variability in addition to volumetric variability and therefore do not directly correspond to the volumes of the individual BNST tracings. Next, the 4 3T thresholded masks (percent overlap: 10/25/50/75) were compared to the original 7T BNST image to determine whether the 3T T2W images could be used as effectively as 7T images. The 3T mask thresholded at 10% had the best overlap with the 7T mask (see Figure 3) and a Dice coefficient of 0.74. As expected, there are some minor differences based on individual variability.

4. DISCUSSION

To our knowledge, this is the first protocol for manual segmentation of the BNST at 3T field strength. Through the utilization of a special T2-weighted MRI sequence, we were able to reliably trace the human BNST. These reliability estimates are comparable to those reported for the manual segmentation of other subcortical regions, such as the pallidum (Fischl et al.,

2002). Furthermore, the resulting 3T BNST mask overlaps well with the previously published 7T mask (Avery et al., 2014), suggesting that the BNST can be successfully and validly traced at the lower 3T field strength.

While there was large overlap in the BNST location across the healthy subjects in this sample, there was also notable variability, which is of concern for patient populations. For example, use of a standardized BNST mask might be difficult in disorders such as schizophrenia in which enlarged lateral ventricles are commonly observed (Haijma et al., 2013). Because this protocol is based on anatomical landmarks, it can be easily adapted for patient populations. Therefore, we recommend that future studies involving patient populations identify subject-specific BNST anatomy through manual tracing in lieu of using standardized masks. Given the inefficiency of manual tracing, future research should focus on developing reliable automatic segmentation routines for the BNST. Although older automated segmentation routines have performed poorly with small subcortical structures, like the amygdala (Morey et al., 2009), newer multi-atlas segmentation methods hold promise (Hanson et al., 2012; Yushkevich et al., 2015).

There were a few limitations involved with this study. First, T2-weighted scans may be more susceptible to motion artifacts than T1-weighted scans (Yushkevich et al., 2015). Second, similar to the amygdala (Entis et al., 2012), the BNST often lacked clear anatomical boundaries and therefore required raters to make subjective decisions. For example, the anterior boundary could vary somewhat by subject and slice thickness. Likewise, the location of the thalamostriate vein near similar veins in the superior portion of the BNST sometimes led to differences in the superior boundary. Finally, although this study demonstrates the ability to trace the BNST as a whole, it should be noted that there are subregions of the BNST that may be functionally distinct and therefore not representative of the entire region (Gungor and Paré, 2016).

In summary, the manual tracing protocol described here provides a practical and reliable method for identifying the BNST on individuals using 3T MRI. Additionally, the BNST mask culminating from the reliability tracings overlays well in healthy human subjects and can be used easily as a simple estimate of the BNST size and location. The method presented here can be integrated easily with functional MRI studies at 3T, laying a critical foundation for increasing scientific knowledge about the human BNST. For example, precise estimates of volume will be important for determining whether BNST size is associated with psychiatric disease, consistent with evidence from other brain regions, such as increased amygdala volume in anxiety vulnerability (Clauss et al., 2014) and decreased hippocampal volume in schizophrenia (Nelson et al., 1998). Furthermore, both the BNST mask generated from this study and the ability to delineate the BNST on individual subjects will provide the necessary tools for 3T imaging to move the field forward.

Supplementary Material

Refer to Web version on PubMed Central for supplementary material.

Acknowledgments

FUNDING

This work was supported by: the US Department of Veterans Affairs (CX001226 to JUB); the National Institute of Mental Health (R21-MH106998 to JUB and R01-MH70560 to SH); the Charlotte and Donald Test Fund; the Vanderbilt Psychiatric Genotype/Phenotype Project; and the Vanderbilt Institute for Clinical and Translational Research (through grant 1-UL-1-TR000445 from the National Center for Research Resources/NIH). The content is solely the responsibility of the authors and does not necessarily represent the official views of the U.S. Department of Veterans Affairs or the National Institutes of Health.

References

Alvarez RP, Chen G, Bodurka J, Kaplan R, Grillon C. Phasic and sustained fear in humans elicits distinct patterns of brain activity. Neuroimage. 2011; 55:389–400. DOI: 10.1016/j.neuroimage.2010.11.057 [PubMed: 21111828]

Avants BB, Epstein CL, Grossman M, Gee JC. Symmetric diffeomorphic image registration with cross-correlation: Evaluating automated labeling of elderly and neurodegenerative brain. Med Image Anal. 2008; 12:26–41. DOI: 10.1016/j.media.2007.06.004 [PubMed: 17659998]

Avery SN, Clauss JA, Blackford JU. The human BNST: functional role in anxiety and addiction. Neuropsychopharmacology. 2016; 41:126–141. DOI: 10.1038/npp.2015.185 [PubMed: 26105138]

Avery SN, Clauss JA, Winder DG, Woodward N, Heckers S, Blackford JU. BNST neurocircuitry in humans. Neuroimage. 2014; 91:311–323. DOI: 10.1016/j.neuroimage.2014.01.017 [PubMed: 24444996]

Banihashemi L, Sheu LK, Midei AJ, Gianaros PJ. Childhood physical abuse predicts stressor-evoked activity within central visceral control regions. Soc Cogn Affect Neurosci. 2013; 10:474–485. DOI: 10.1093/scan/nsu073

Choi JM, Padmala S, Pessoa L. Impact of state anxiety on the interaction between threat monitoring and cognition. Neuroimage. 2012; 59:1912–1923. DOI: 10.1016/j.neuroimage.2011.08.102 [PubMed: 21939773]

Clauss JA, Seay AL, Vanderklok R, Avery S, Cao A, Cowan RL, Benningfield MM, Blackford JU. Structural and functional bases of inhibited temperament. Soc Cogn Affect Neurosci. 2014; 9:2049–2058. [PubMed: 24493850]

Davis M, Walker DL, Lee Y. Amygdala and bed nucleus of the stria terminalis: differential roles in fear and anxiety measured with the acoustic startle reflex. Philos Trans Biol Sci. 1997; 352:1675–1687. DOI: 10.1098/rstb.1997.0149

Davis M, Walker DL, Miles L, Grillon C. Phasic vs sustained fear in rats and humans: role of the extended amygdala in fear vs anxiety. Neuropsychopharmacology. 2010; 35:105–135. DOI: 10.1038/npp.2009.109 [PubMed: 19693004]

Dice LR. Measures of the amount of ecologic association between species. Ecology. 1945; 26:297–302.

Entis JJ, Doerga P, Barrett LF, Dickerson BC. A reliable protocol for the manual segmentation of the human amygdala and its subregions using ultra-high resolution MRI. Neuroimage. 2012; 60:1226–1235. [PubMed: 22245260]

Fedorov A, Beichel R, Kalpathy-Cramer J, Finet J, Fillion-Robin JC, Pujol S, Bauer C, Jennings D, Fennessy F, Sonka M, Buatti J, Aylward S, Miller JV, Pieper S, Kikinis R. 3D Slicer as an image computing platform for the Quantitative Imaging Network. Magn Reson Imaging. 2012; 30:1323–41. DOI: 10.1016/j.mri.2012.05.001 [PubMed: 22770690]

First, MB., Spitzer, RL., Gibbon, M., Williams, JBW. Biometrics Research. New York State Psychiatric Institute; New York: 2002. Structured Clinical Interview For DSM-IV-TR Axis I Disorders, Research Version, Patient Edition (SCID-I/P).

Fischl B, Salat DH, Busa E, Albert M, Dieterich M, Haselgrove C, van der Kouwe A, Killiany R, Kennedy D, Klaveness S, Montillo A, Makris N, Rosen B, Dale AM. Whole Brain Segmentation: Neurotechnique Automated Labeling of Neuroanatomical Structures in the Human Brain. Neuron. 2002; 33:341–355. DOI: 10.1016/S0896-6273(02)00569-X [PubMed: 11832223]

Grupe DW, Oathes DJ, Nitschke JB. Dissecting the anticipation of aversion reveals dissociable neural networks. Cereb Cortex. 2013; 23:1874–83. DOI: 10.1093/cercor/bhs175 [PubMed: 22763169]

Gungor NZ, Paré D. Functional Heterogeneity in the Bed Nucleus of the Stria Terminalis. J Neurosci. 2016; 36:8038–49. DOI: 10.1523/JNEUROSCI.0856-16.2016 [PubMed: 27488624]

Haijma SV, Van Haren N, Cahn W, Koolschijn PCMP, Hulshoff Pol HE, Kahn RS. Brain volumes in schizophrenia: A meta-analysis in over 18 000 subjects. Schizophr Bull. 2013; 39:1129–1138. DOI: 10.1093/schbul/sbs118 [PubMed: 23042112]

Hanson JL, Suh JW, Nacewicz BM, Sutterer MJ, Cayo AA, Stodola DE, Burghy CA, Wang H, Avants BB, Yushkevich PA, Essex MJ, Pollak SD, Davidson RJ. Robust automated amygdala segmentation via multi-atlas diffeomorphic registration. Front Neurosci. 2012; 6:166.doi: 10.3389/fnins.2012.00166 [PubMed: 23226114]

Herrmann MJ, Boehme S, Becker MPI, Tupak SV, Guhn A, Schmidt B, Brinkmann L, Straube T. Phasic and sustained brain responses in the amygdala and the bed nucleus of the stria terminalis during threat anticipation. Hum Brain Mapp. 2016; 37:1091–1102. DOI: 10.1002/hbm.23088 [PubMed: 26678871]

Jenkinson M, Smith S. A global optimisation method for robust affine registration of brain images. Med Image Anal. 2001; 5:143–156. DOI: 10.1016/S1361-8415(01)00036-6 [PubMed: 11516708]

Jennings JH, Sparta DR, Stamatakis AM, Ung RL, Pleil KE, Kash TL, Stuber GD. Distinct extended amygdala circuits for divergent motivational states. Nature. 2013; 496:224–228. DOI: 10.1038/nature12041 [PubMed: 23515155]

Kash TL. The role of biogenic amine signaling in the bed nucleus of the stria terminals in alcohol abuse. Alcohol. 2012; 46:303–308. DOI: 10.1016/j.alcohol.2011.12.004 [PubMed: 22449787]

Klumpers F, Kroes MC, Heitland I, Everaerd D, Akkermans SEa, Oosting RS, van Wingen G, Franke B, Kenemans JL, Fernández G, Baas JMP. Dorsomedial prefrontal cortex mediates the impact of serotonin transporter linked polymorphic region genotype on anticipatory threat reactions. Biol Psychiatry. 2015; 78:582–589. DOI: 10.1016/j.biopsych.2014.07.034 [PubMed: 25444169]

Koob GF, Volkow ND. Neurocircuitry of addiction. Neuropsychopharmacology. 2010; 35:217–38. DOI: 10.1038/npp.2009.110 [PubMed: 19710631]

Mai, JK., Maijtanik, M., Paxinos, G. Atlas of the Human Brain. 4. Academic Press; New York: 2015.

Mcmenamin BW, Langeslag SJE, Sirbu M, Padmala S, Pessoa XL. Network organization unfolds over time during periods of anxious anticipation. J Neurosci. 2014; 34:11261–11273. DOI: 10.1523/JNEUROSCI.1579-14.2014 [PubMed: 25143607]

Mobbs D, Yu R, Rowe JB, Eich H, FeldmanHall O, Dalgleish T. Neural activity associated with monitoring the oscillating threat value of a tarantula. Proc Natl Acad Sci U S A. 2010; 107:20582–20586. DOI: 10.1073/pnas.1009076107 [PubMed: 21059963]

Morey RA, Petty CM, Xu Y, Hayes JP, Wagner HR, Lewis DV, LaBar KS, Styner M, McCarthy G. A comparison of automated segmentation and manual tracing for quantifying hippocampal and amygdala volumes. Neuroimage. 2009; 45:855–66. DOI: 10.1016/j.neuroimage.2008.12.033 [PubMed: 19162198]

Motzkin JC, Philippi CL, Oler JA, Kalin NH, Baskaya MK, Koenigs M. Ventromedial prefrontal cortex damage alters resting blood flow to the bed nucleus of stria terminalis. Cortex. 2015; 64:281–288. DOI: 10.1016/j.cortex.2014.11.013 [PubMed: 25569763]

Münsterkötter AL, Notzon S, Redlich R, Grotegerd D, Dohm K, Arolt V, Kugel H, Zwanzger P, Dannlowski U. Spider or no spider? neural correlates of sustained and phasic fear in spider phobia. Depress Anxiety. 2015; 32:656–663. DOI: 10.1002/da.22382 [PubMed: 26115440]

Nelson MD, Saykin AJ, Flashman LA, Riordan HJ. Hippocampal volume reduction in schizophrenia as assessed by magnetic resonance imaging. Arch Gen Psychiatry. 1998; 55:433–440. [PubMed: 9596046]

Schlund MW, Hudgins CD, Magee S, Dymond S. Neuroimaging the temporal dynamics of human avoidance to sustained threat. Behav Brain Res. 2013; :1–8. DOI: 10.1016/j.bbr.2013.09.042

Shackman AJ, Fox AS. Contributions of the Central Extended Amygdala to Fear and Anxiety. J Neurosci. 2016; 36:8050–8063. DOI: 10.1523/JNEUROSCI.0982-16.2016 [PubMed: 27488625]

Somerville LH, Wagner DD, Wig GS, Moran JM, Whalen PJ, Kelley WM. Interactions between transient and sustained neural signals support the generation and regulation of anxious emotion. Cereb Cortex. 2013; 23:49–60. DOI: 10.1093/cercor/bhr373 [PubMed: 22250290]

Somerville LH, Whalen PJ, Kelley WM. Human bed nucleus of the stria terminalis indexes hypervigilant threat monitoring. Biol Psychiatry. 2010; 68:416–24. DOI: 10.1016/j.biopsych.2010.04.002 [PubMed: 20497902]

Stamatakis AM, Sparta DR, Jennings JH, McElligott Za, Decot H, Stuber GD. Amygdala and bed nucleus of the stria terminalis circuitry: Implications for addiction-related behaviors. Neuropharmacology. 2014; 76:320–328. DOI: 10.1016/j.neuropharm.2013.05.046 [PubMed: 23752096]

Straube T, Mentzel HJ, Miltner WHR. Waiting for spiders: Brain activation during anticipatory anxiety in spider phobics. Neuroimage. 2007; 37:1427–1436. [PubMed: 17681799]

Torrisi S, O'Connell K, Davis A, Reynolds R, Balderston N, Fudge JL, Grillon C, Ernst M. Resting state connectivity of the bed nucleus of the stria terminalis at ultra-high field. Hum Brain Mapp. 2015; 36:4076–4088. DOI: 10.1002/hbm.22899 [PubMed: 26178381]

Walker DL, Toufexis DJ, Davis M. Role of the bed nucleus of the stria terminalis versus the amygdala in fear, stress, and anxiety. Eur J Pharmacol. 2003; 463:199–216. DOI: 10.1016/S0014-2999(03)01282-2 [PubMed: 12600711]

Yassa, Ma, Hazlett, RL., Stark, CEL., Hoehn-Saric, R. Functional MRI of the amygdala and bed nucleus of the stria terminalis during conditions of uncertainty in generalized anxiety disorder. J Psychiatr Res. 2012; 46:1045–52. DOI: 10.1016/j.jpsychires.2012.04.013 [PubMed: 22575329]

Yushkevich PA, Pluta JB, Wang H, Xie L, Ding SL, Gertje EC, Mancuso L, Kliot D, Das SR, Wolk DA. Automated volumetry and regional thickness analysis of hippocampal subfields and medial temporal cortical structures in mild cognitive impairment. Hum Brain Mapp. 2015; 36:258–287. DOI: 10.1002/hbm.22627 [PubMed: 25181316]

Yushkevich PA, Wang H, Pluta J, Das SR, Craige C, Avants BB, Weiner MW, Mueller S. Nearly automatic segmentation of hippocampal subfields in in vivo focal T2-weighted MRI. Neuroimage. 2010; 53:1208–1224. DOI: 10.1016/j.neuroimage.2010.06.040 [PubMed: 20600984]

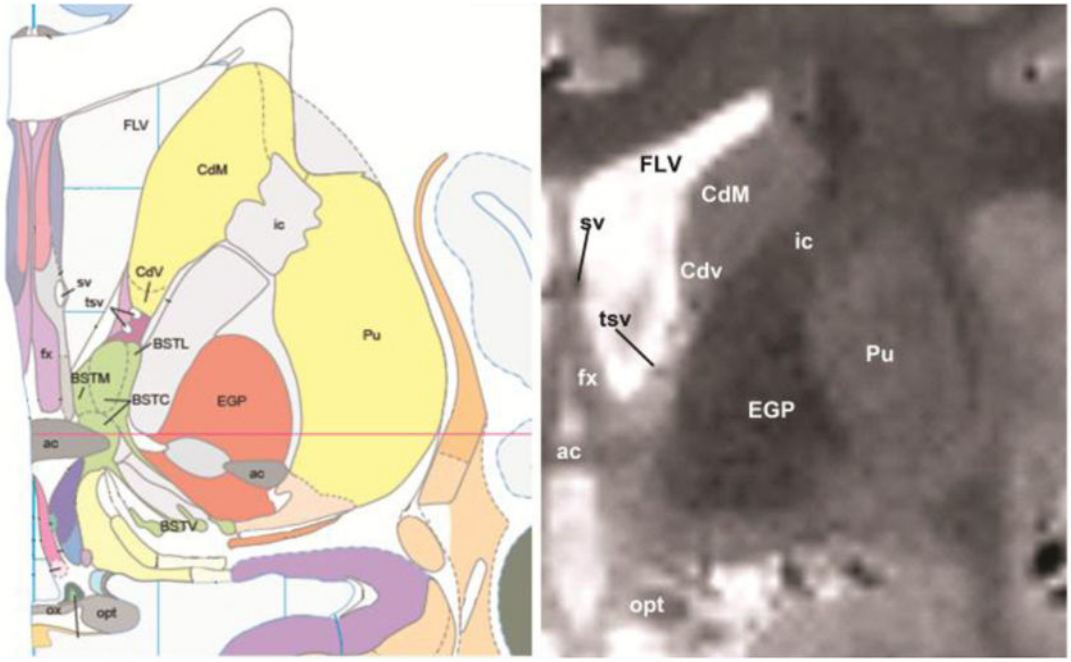

Figure 1. Structural MRI scan of the human BNST

The anatomical location of the human BNST (left: Mai atlas, right: T2W MRI scan). Abbreviations: ac = anterior commissure; BST (BSTM, BSTC, BSTV) = bed nucleus of the stria terminals; Cd (CdM and Cdv) = caudate; EGP = external globus pallidus; FLV = frontal horn of the lateral ventricle; fx = fornix; ic = internal capsule; opt = optic nerve; ox = optic chiasm; Pu = putamen; tsv = thalamostriate vein.

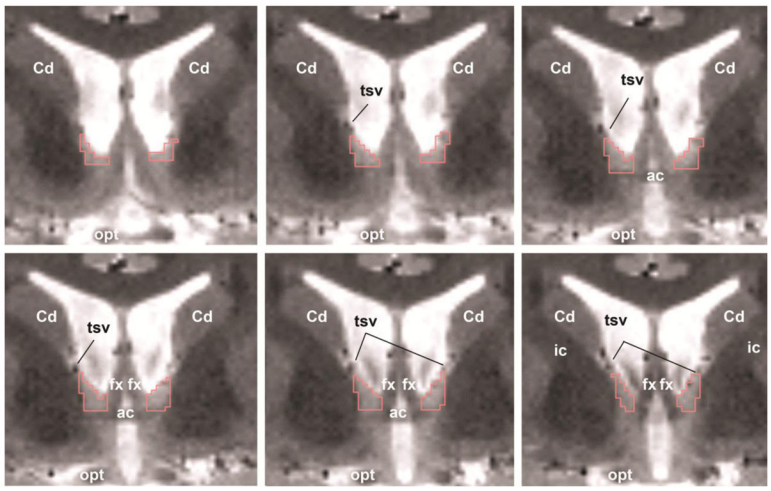

Figure 2. Delineation of the human BNST

The BNST is identified by the red boundary (voxel size 0.8 mm × 0.8 mm × 0.9 mm) moving from the anterior (top left) to the posterior (bottom right). Cd = caudate, tsv = thalamostriate vein, ac = anterior commissure, ic = internal capsule, fx = fornix, opt = optic nerve.

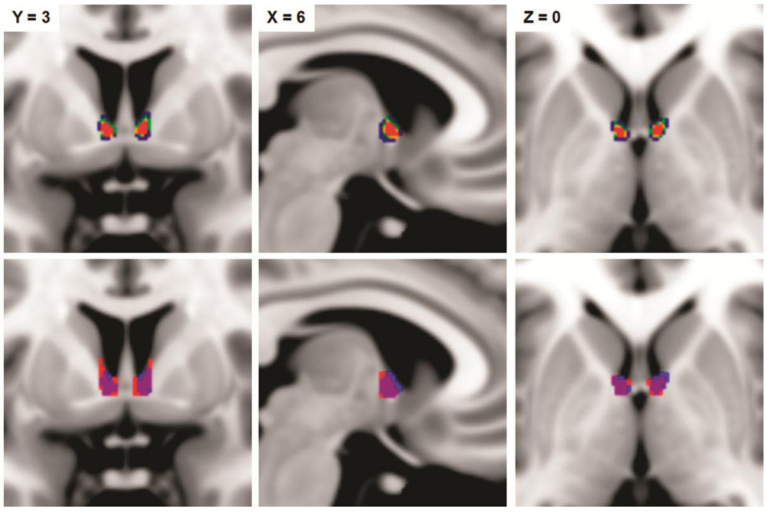

Figure 3. Probabilistic BNST mask

Top row: Probabilistic mask of the BNST (blue=10%, green=25%, yellow=50%, and red=75% overlap). Bottom row: Overlay of Avery et al. (2014) 7T BNST mask (red) and the 3T mask thresholded at 10% (blue) on an averaged T1 MNI brain. Violet areas demonstrate the overlap of the two masks.